Understanding the Uncertainty in the West African Monsoon Precipitation Response to Increasing CO_2

Harry Mutton, [a] Robin Chadwick, [a,b] Matthew Collins, [b] F. Hugo Lambert, [b], Christopher M. Taylor, [c,d] Ruth Geen, [e] Hervé Douville, [f] Marion Saint-Lu [g]

[a] *Met Office Hadley Centre, Exeter, UK*

[b] *University of Exeter, Exeter, UK*

[c] *UK Centre for Ecology and Hydrology, Wallingford, UK*

[d] *National Centre for Earth Observations, Wallingford, UK*

[e] *University of Birmingham, Birmingham, UK*

[f] *Centre National de Recherches Météorologiques, Météo-France/CNRS, Toulouse, France*

[g] *Laboratoire de Météorologie Dynamique (LMD)/Institut Pierre Simon Laplace (IPSL), Sorbonne Université/CNRS/École Normale Supérieure/École Polytechnique, Paris, France*

Corresponding author: Harry Mutton, harry.mutton@metoffice.gov.uk

Early Online Release: This preliminary version has been accepted for publication in *Journal of Climate*, may be fully cited, and has been assigned DOI 10.1175/JCLI-D-24-0506.1. The final typeset copyedited article will replace the EOR at the above DOI when it is published.

ABSTRACT: The West African Monsoon (WAM) precipitation response to increased CO_2 is uncertain, with both large increases and decreases predicted by CMIP6 models. To address this, the full impact of increased CO_2 has been decomposed into several drivers, three of which are shown to contribute most to the uncertainty in the WAM precipitation response; the direct radiative effect of increased CO_2, the impact of a uniform Sea Surface Temperature (SST) warming, and the impact of a patterned SST change. Much of the uncertainty associated with the response to the direct radiative effect and uniform SST warming is shown to be related to differing changes in 700hPa moisture flux divergence associated with the shallow meridional circulation over West Africa as well as differences in a soil moisture - surface heat flux feedback over the Sahel. For the SST pattern effect, the difference between North Atlantic SSTs and tropical mean SSTs, as well as inter-hemispheric gradients in surface temperatures are key drivers of intermodel spread. Suggestions for how to reduce uncertainty in the response are discussed.

1. Introduction

Due to their substantial social and economic significance, understanding how regional monsoons are projected to change in the future is of great importance (e.g. Akinsanola and Zhou (2020), Raj et al. (2019), Sahastrabuddhe et al. (2023), and Katzenberger et al. (2021)). In the Intergovernmental Panel on Climate Change Sixth Assessment Report (IPCC AR6) it was shown that compared to other monsoon regions, West African monsoon (WAM) precipitation projections are much less certain, particularly for long term high emission scenarios (Masson-Delmotte et al. (2021) and references therein). Given the WAM supports millions of people and sustains a large agricultural sector in the region, understanding how WAM precipitation is likely to change in the future is of high importance and is key to providing suitable and well informed adaptation policies (Cook and Vizy 2019; Raj et al. 2019).

To better understand this uncertainty in WAM precipitation projections, a variety of approaches have previously been taken. Monerie et al. (2020b) decomposed the Coupled Model Intercomparison Project (CMIP5 and CMIP6) intermodel precipitation uncertainty into dynamic and thermodynamic components. The thermodynamic component represents differences in moisture availability, which is expected to increase in a warmer climate (Chadwick et al. 2016), whilst the dynamic component represents the different atmospheric circulation responses across models. It was shown that much of the intermodel uncertainty results from the dynamic term, which Monerie et al. (2020b) linked to the atmospheric response to changes in Sea Surface Temperatures (SST)s, particularly over the North Atlantic.

Understanding uncertainty in WAM projections caused by SST patterns is particularly challenging, since there is uncertainty caused by the different SST patterns projected by models as well as differing model responses to a given SST pattern change. Guilbert et al. (2024) employed metrics for both inter-hemispheric asymmetry in warming and tropical pacific warming to explain uncertainty in WAM projections. They show that these SST patterns influence the WAM through shifts in the ITCZ and Walker Circulation respectively. Monerie et al. (2023) investigated intermodel uncertainty with a "storylines" approach showing that both warming in the North Atlantic and the Mediterranean contribute to increased WAM precipitation in the future, consistent with Park et al. (2016). Park et al. (2015) investigated the influence of differential warming between

Accepted for publication in *Journal of Climate*. DOI 10.1175/JCLI-D-24-0506.1.

NH tropics and extratropics. Giannini et al. (2013) developed an index whereby both past WAM variability and differing future projections in WAM precipitation could be understood through the difference between North Atlantic and tropical mean SSTs. They noted that the tropical mean SSTs play an important role in setting the vertical atmospheric stability across the tropics and setting the temperature threshold for deep convection (Johnson and Xie 2010). Provided sufficiently high temperature and moisture conditions are met in the lower troposphere and this threshold is exceeded, convection can occur. Since the Atlantic is a key moisture source for the WAM (Lele et al. 2015; Gong and Eltahir 1996), the Atlantic SSTs play an important role in determining to what extent this convective threshold is met in the WAM region. Giannini et al. (2013) focus more specifically on the North Atlantic SSTs as being the most relevant to the WAM, finding strong correlations between monsoon precipitation and the difference between North Atlantic and tropical mean SSTs across a range of timescales and across different models. Bellomo et al. (2021) showed that variability in North Atlantic SSTs is related to differing projections of the AMOC, and the SSTs caused by this AMOC variability have large impacts on the latitudinal displacement of the ITCZ and the mid-latitude jet.

Land-atmosphere coupling has also been found to be a key source of uncertainty. Dosio et al. (2020) took a different approach to understanding the key differences in models' WAM projections under the RCP8.5 emissions scenario. Regional climate models were used to downscale six CMIP5 GCMs and these models were grouped into 'wet' and 'dry' classifications, where the 'wet' models were those that projected an increase in West African precipitation and the 'dry' models were those that projected a decrease. This grouping highlighted that a key difference between wet and dry models was associated with land–atmosphere coupling, with large discrepancies in soil moisture and evapotranspiration changes between the two groups. Mutton et al. (2022) and Mutton et al. (2023) demonstrated that a soil moisture - surface heat flux feedback over the Sahel can act to amplify any increases or decreases in WAM precipitation. It is possible that this feedback mechanism could be a key contributor to the model diversity highlighted by Dosio et al. (2020).

Previously, Mutton et al. (2022, 2023) employed a decomposition of the full coupled atmosphere-ocean model response to increasing CO2 into a number of direct and indirect drivers such as the direct radiative effect or a uniform ocean warming to better understand the mechanisms responsible

for changes in WAM precipitation. Using this decomposition it was shown that in response to the direct radiative effect of increased CO_2, the WAM precipitation increases (Mutton et al. 2022; Gaetani et al. 2017; Chadwick et al. 2019; Biasutti 2019). This increase was shown to be caused by differential heating between the moist monsoon air mass and the drier desert air mass to the north, generating a weakening and a northward shift in the shallow meridional circulation which climatologically tends to advect dry air in to the monsoon rainband at midlevels and inhibit precipitation (Shekhar and Boos 2017; Zhang et al. 2008). It was also shown that a local soil moisture-surface heat flux feedback over the Sahel acted to amplify circulation changes and determine the location of the inter-tropical discontinuity (Mutton et al. 2022). The mechanism discussed in Mutton et al. (2022) has been summarised in Figure 1a. Investigating the WAM response to a uniform ocean warming, shown to cause a decrease in WAM precipitation (Hill et al. 2017; Held et al. 2005; Gaetani et al. 2017; Biasutti 2013, 2019), Mutton et al. (2023) demonstrated that this decrease in WAM precipitation was caused by a strengthening of the 700hPa moisture flux divergence associated with the shallow meridional circulation (due to the effect of both increased moisture gradients over the Sahel and a strengthening of the circulation itself), and a southward shift in the African Easterly Jet. Similar to the direct radiative effect mechanism discussed, a soil moisture-surface heat flux feedback over the Sahel also acts to amplify changes in circulation and precipitation. These mechanisms have been summarised in Figure 1b. Gaetani et al. (2017) also used a similar decomposition, suggesting that the spread in projections may be caused by the balance of the WAM response to the opposing signals from the direct radiative effect and a uniform ocean warming.

Building on the mechanistic understanding provided by Mutton et al. (2022) and Mutton et al. (2023), as well as the SST pattern effect understanding provided by Giannini et al. (2013) and Guilbert et al. (2024), in this paper we employ the decomposition used by Mutton et al. (2023) to better understand the different sources of uncertainty in the WAM precipitation response to increased CO_2 across the CMIP6 ensemble. Using such a decomposition simplifies the response to increased CO_2 and allows us to isolate the uncertainty in projections associated with different components of the response. Here the direct radiative effect, the uniform ocean warming, and the patterned SST change are shown to be the largest source of uncertainty, and it is shown that the mechanisms found to be responsible for WAM precipitation changes in Mutton et al. (2022)

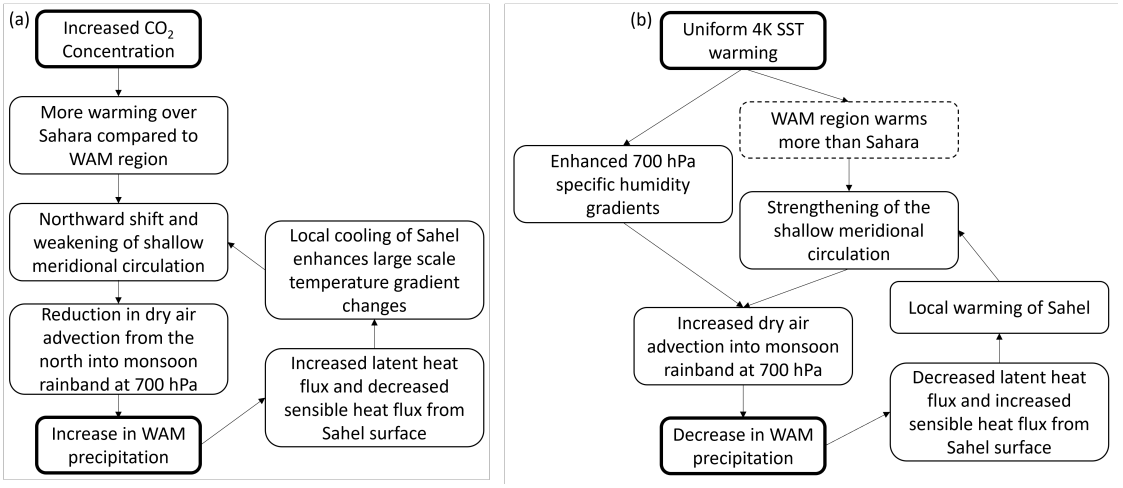

FIG. 1. Diagram depicting the key processes responsible for (a) an increase in WAM precipitation in response to the direct radiative effect of increased CO_2, and (b) a decrease in WAM precipitation in response to a uniform ocean warming (Mutton et al. 2022, 2023). Here the dashed line around the box in (b) highlights the fact that this feature was predominantly present in an adjustment period over the days following an abrupt ocean warming. There is some evidence that the warming pattern mentioned is seen in the long term steady state response to ocean warming, particularly prior to the onset of the monsoon season, but more work is needed to investigate this further (Mutton et al. 2023).

and Mutton et al. (2023), in particular those associated with the shallow meridional circulation, may also contribute to the large spread in WAM projections. The uncertainty associated with the patterned SST change is investigated, using the indices developed by Giannini et al. (2013) and Guilbert et al. (2024), specifically the difference between North Atlantic and Tropical SSTs and the inter-hemispheric asymmetry in surface temperatures.

Section 2 describes the data and methods used, and section 3 presents the results. The results have been split into four sub-sections where section 3a presents the decomposition used, Section 3b investigates the intermodel spread associated with the direct radiative effect, section 3c investigates the intermodel spread associated with a uniform SST change, and section 3d investigates the intermodel spread associated with a patterned SST change. Finally, a discussion and conclusions are presented in section 4.

2. Data and Methods

a. Experiment design

Two different experimental setups are used to isolate the different components of the response to the full forcing of increased CO_2. This response to the full forcing of increased CO_2 is defined as the difference between piControl and abrupt-4xCO2 experiments, where the piControl experiment is a coupled model experiment with pre-industrial atmospheric constituents and the abrupt-4xCO2 experiment is a coupled model experiment where the CO_2 concentrations have been abruptly quadrupled relative to pre-industrial levels. The more accurate and comprehensive of the two decompositions used involves the CMIP6 piSST timeslice experiments. The piSST experiment is an atmosphere only experiment that uses pre-industrial atmospheric constituents and prescribed monthly varying SST from years 111 – 140 of the models own piControl simulation. piSST-4xCO2-rad is similar to piSST except the CO_2 concentrations seen by the radiation scheme have been multiplied by 4. Since this increase in CO_2 is only seen by the radiation scheme there are no changes due to the plant physiology response to increased CO_2. The difference between piSST-4xCO2-rad and piSST gives the direct radiative effect. The piSST-4xCO2 experiment is identical to the piSST-4xCO2-rad experiment except the increase in CO_2 is seen by both the vegetation and radiation scheme. Taking the difference between these two experiments provides the plant physiological effect which captures the response to changes in plant stomata, which tend to close with increased CO_2, as well as changes in leaf area index in some models (Chadwick et al. 2019). The piSST-pxK experiment is similar to the piSST experiment however here a uniform SST warming has been applied. The magnitude of this SST warming is calculated as the global climatological mean change in SSTs between years 111 – 140 of the model's own piControl and abrupt-4xCO2 experiments. The difference between piSST-p4K and piSST provides the impact of a uniform ocean warming. The a4SST experiment is also similar to the piSST experiment but has monthly varying SSTs prescribed from years 111-140 of the model's own abrupt-4xCO2 experiment. Taking the difference between a4SST and piSST-p4K provides the impact of a patterned SST change. a4SSTice is similar to the a4SST experiment but also has monthly varying sea ice prescribed from the models own abrupt-4xCO2 experiment. Comparing a4SST and a4SSTice provides the impact of changing sea ice. Finally a4SSTice-4xCO2 is similar to the a4SSTice experiment but also has the CO_2

Timeslice Experiments			
Experiment Name	Prescribed SSTs	CO_2 Concentrations	Sea Ice
piSST	piControl	Preindustrial	piControl
piSST-4xCO2-rad	piControl	Preindustrial × 4 (increase only seen by the radiation scheme)	piControl
piSST-4xCO2	piControl	Preindustrial × 4	piControl
piSST-pxK	piControl + global mean SST anomaly from abrupt-4xCO2 - piControl	Pre-industrial	piControl
a4SST	abrupt-4xCO2	Preindustrial	piControl
a4SSTice	abrupt-4xCO2	Preindustrial	abrupt-4xCO2
a4SSTice-4xCO2	abrupt-4xCO2	Preindustrial × 4	abrupt-4xCO2

TABLE 1. Description of experimental set-up for piSST based timeslice experiments used to decompose the abrupt-4xCO2 response. All experiments are run for 30 years. 4 models have simulated these experiments.

Timeslice Component Definition
Direct Radiative Effect = piSST-4xCO2-rad - piSST
Uniform SST Warming = piSST-pxK - piSST
Patterned SST Change = a4SST - piSST-pxK
Plant Effect = piSST-4xCO2 - piSST-4xCO2-rad
Sea Ice Effect = a4SSTice - a4SST
Full AGCM = a4SSTice-4xCO2 - piSST
Residual / Non-linear = Full AGCM - Sea Ice Effect - Plant Effect - Patterned SST Change - Uniform SST Warming - Direct Radiative Effect
Coupled = abrupt-4xCO2 - piControl

TABLE 2. Definition of components of full forcing of increased CO_2 using timeslice experiments. Decomposition presented in Figure 3 and 4 and experimental setup described in Table 1.

concentrations set to 4 times pre-industrial levels seen by both the vegetation and radiation scheme. Comparing a4SSTice-4xCO2 and piSST captures the atmosphere-only model's full response to increased CO_2. The experimental setup of these timeslice experiments are summarised in Table 1, and the different components of the full response are calculated as stated in Table 2 (Chadwick et al. 2017). The experimental set-up is also described in Webb et al. (2017). This decomposition is discussed further in section 3a.

Although these piSST timeslice experiments do give a comprehensive decomposition of the full response to increased CO_2, across CMIP6, only 4 models have performed these simulations. Therefore, to capture the responses to different components of the full CO_2 forcing in a larger ensemble of models, amip, amip-4xCO2, and amip-p4K experiments are used (Table 3). The amip

amip Experiments			
Experiment Name	Prescribed SSTs	CO_2 Concentrations	Sea Ice
amip	Historical	Historical	Historical
amip-4xCO2	Historical	Historical × 4 (only seen by the radiation scheme)	Historical
amip-p4K	Historical + 4K	Historical	Historical

TABLE 3. Description of experimental set-up for amip experiments used. Each experiment runs from 1979 – 2014. 13 models have simulated these experiments.

experiment is an AGCM experiment forced by observed historical SSTs, sea ice, and atmospheric constituents between 1979 and 2014. The amip-4xCO2 uses an identical setup, only the CO_2 concentrations are multiplied by 4, and this increase in CO_2 is only seen by the radiation scheme, therefore causing no changes to plant physiology. In the case of amip-p4K, this also uses an identical setup to amip, only a uniform warming of 4K is applied to the SSTs. The impact of the direct radiative effect of increased CO_2 is isolated by taking the difference between amip-4xCO2 and amip experiments, and the impact of a uniform ocean warming is calculated as the difference between amip-p4K and amip experiments. This decomposition has previously been used by Monerie et al. (2020a), Gaetani et al. (2017), Mutton et al. (2022) and Mutton et al. (2023).

13 models have run the amip based experiments shown in Table 3; CESM2, BCC-CM2-MR, CNRM-CM6-1, HadGEM3-GC31-LL, IPSL-CMA6A-LR, MRI-ESM2-0, CanESM5, MIROC6, GISS-E2-1-G, GFDL-CM4, TaiESM1, E3SM-1-0, and NorESM2-LM. 4 models have run the timeslice experiments described in Table 1; HadGEM3-GC31-LL, IPSL-CM6A-LR, CESM2, and CNRM-CM6-1. In both sets of experiments 1 ensemble member of each simulation was used. In figures where multi-model means have been calculated, data have been regridded onto a 1.85°longitude by 1.25°latitude grid. All model data used in this analysis are accessible from the ESGF CMIP6 site (Eyring et al. 2016).

b. Regions Analysed

Consistent with the analysis of Shekhar and Boos (2017), Mutton et al. (2022), and Mutton et al. (2023), much of the analysis focuses on a cross section of the atmosphere, zonally averaging between 10°W to 25°E (Figure 2 green lines). The WAM region (Figure 2 dark blue box) is defined

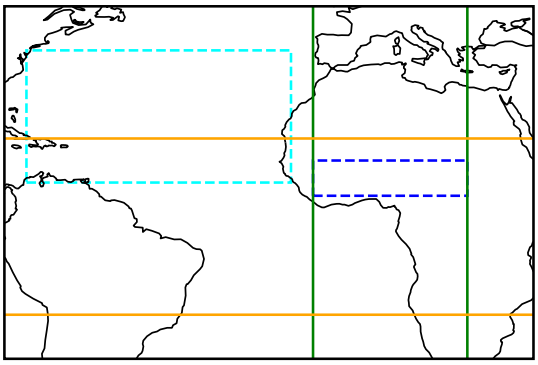

FIG. 2. Regions used for analysis; green lines indicate the longitudinal bounds used for cross-section analysis and the dashed dark blue box indicates West African monsoon region. Dashed cyan box indicates the region used to characterise the North Atlantic SSTs and the orange lines indicate the latitudinal bounds used to calculate tropical mean SSTs.

as a region between 10°W to 25°E and 7 to 15°N. This box captures much of the region where the June–August precipitation minus December–February precipitation is greater than 180mm and the June–August precipitation accounts for over 35% of the total annual rainfall in GPCP observations between 1980 and 2010. These criteria are used by Wang and Ding (2006) to characterise monsoon regions. The cyan box and the orange lines are used to define northern tropical Atlantic SSTs and Tropical Mean surface temperatures respectively, as used by Giannini et al. (2013) to calculate their index for capturing WAM variability in response to changing SST patterns.

c. Definition of Key Quantities

1) Low Level Atmospheric Thickness (LLAT)

LLAT is defined as the difference between 700hPa and 925hPa geopotential heights (Equation 1) (Lavaysse et al. 2009; Shekhar and Boos 2017).

$$\text{LLAT} = Z_g(700hPa) - Z_g(925hPa) \tag{1}$$

where $Z_g(p)$ is the geopotential height at pressure p. LLAT is used here to document changes in the Saharan heat low and the shallow meridional circulation over West Africa.

2) Horizontal Divergences

Horizontal divergence of moisture flux is used to capture changes in the shallow meridional circulation over West Africa and is defined using Equation 2.

$$\text{Horizontal divergence of moisture flux} = \nabla_h \cdot qV \tag{2}$$

Where V is the wind, q is the specific humidity, and $\nabla_h \cdot$ is the horizontal divergence operator. Here, only the 700hPa moisture flux divergence has been analysed.

Changes in horizontal divergence of moisture transport can be decomposed into dynamic and thermodynamic components using Equations 3 and 4 respectively (Endo and Kitoh 2014; Dosio et al. 2020).

$$\Delta_{Dynamic}(\nabla_h \cdot qV) = \nabla_h \cdot (q_A \Delta V) \tag{3}$$

$$\Delta_{Thermodynamic}(\nabla_h \cdot qV) = \nabla_h \cdot (V_A \Delta q) \tag{4}$$

Where subscript A refers to the amip experiment and Δ refers to the difference between the initial and resulting state.

Ideally the analysis of horizontal moisture flux divergence would be performed using high temporal resolution (6 hourly) data (Seager et al. 2014). However, due to incomplete data availability in even daily data, monthly data has been used. To demonstrate the impact of using this coarser temporal resolution data, a comparison between monthly and daily data has been provided in Figure S1. This shows that although this caveat should be taken into consideration, it would not likely alter the conclusions drawn from the results.

3. Results

The results of this analysis have been split into four sections. Firstly, in Section 3a, the WAM precipitation decomposition using the piSST based and amip based experiments is presented and the relative importance of each driver of WAM precipitation change to the intermodel spread in projections is shown. It is found that the largest contributions to intermodel spread come from the different responses to the direct radiative effect, the uniform ocean warming, and a patterned SST change. Section 3b, 3c, and 3d then investigate these components further applying the results

of Mutton et al. (2022), Mutton et al. (2023), Giannini et al. (2013) and Guilbert et al. (2024) respectively, to investigate whether the mechanisms previously shown to drive WAM precipitation change in response to these drivers are also key to understanding the spread in model projections seen across a subset of CMIP6 models.

a. Timeslice Decomposition

WAM precipitation change in response to a quadrupling of CO_2 in the abrupt-4xCO2 experiment as well as the decomposition of this change using the piSST and amip based experiments is shown in Figure 3. As previously mentioned, the spread in the abrupt-4xCO2 response is substantial, with both large increases and large decreases seen across the 41 model CMIP6 ensemble (Figure 3 box plot). The large WAM precipitation decrease seen in some of the more extreme models is particularly policy relevant and would have substantial socioeconomic impacts were such a decrease to occur, emphasising the importance of improving projections in WAM precipitation.

Decomposing the abrupt-4xCO2 response into the different components demonstrates that the direct radiative effect of increased CO_2 causes an increase in WAM precipitation, the uniform SST warming causes a decrease in WAM precipitation, and the response to a patterned SST change is uncertain, with a comparable spread across the 4 piSST models to that seen in response to the direct radiative effect or uniform SST warming. The spread in the response to sea ice melt or changing plant physiology is small compared to that of the direct radiative effect, uniform SST warming, and patterned SST changes, as is the spread in the residual term which includes the nonlinearities in the decomposition. The direct radiative effect and uniform SST warming responses are also shown for the amip based decomposition and the associated abrupt-4xCO2 response for this ensemble is indicated. The increased ensemble size (13 models) compared to the 4 model ensemble for the piSST decomposition helps to capture a greater intermodel spread and also allows us to sample models spanning the entire range of the larger 41 model CMIP6 ensemble.

The spatial characteristics of the response to different components of the piSST decomposition is presented in Figure 4. Consistent with Figure 3, the largest components of the decomposition are the direct radiative effect, the uniform SST warming and the patterned SST change, although the response to the patterned SST change is generally small in three of the four models and large

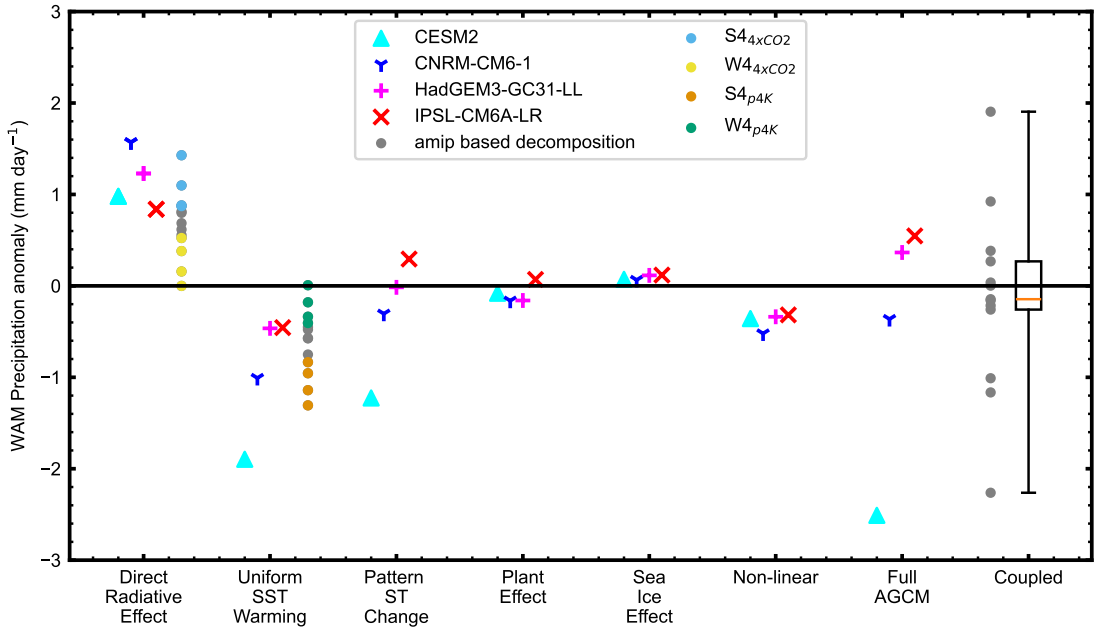

FIG. 3. West African Monsoon precipitation response to different components of the piSST based timeslice decomposition of the full coupled CO_2 response in 4 CMIP6 GCMs (see Table 1 and 2 for description of each component of the decomposition). The coupled response is defined as the difference between piControl and abrupt-4xCO2 experiments. WAM precipitation is defined as the area average precipitation over the blue box indicated in Figure 1 between June-August. Dots alongside the direct radiative effect and uniform SST warming columns indicate the intermodel spread in the 13 model ensemble of amip based experiments (see Table 3). Here the different coloured dots indicate whether it is in the stronger or weaker groups used later in section 3b and 3c. The box plot in the coupled model column indicates the intermodel spread in a 41 member ensemble of CMIP6 models. Lower and upper box boundaries indicate the interquartile range with central horizontal line indicating the median. Whiskers indicate the maximum and minimum values.

and negative in CESM2. Again, the response to changes in sea ice and plants are shown to be small and not significant, and whilst the non-linear term is also small compared to the direct radiative effect and uniform SST change, there are some regions where the small but negative anomalies are significant. Comparing the precipitation changes seen in the full AGCM response and the coupled abrupt-4xCO2 response it can be seen that although there are some regions where small differences in the response emerge, broadly the piSST decomposition does a good job at capturing the coupled abrupt-4xCO2 response with spatial correlations between the two responses ranging from 0.93 to

0.99 across the four models. Given that the non-linear term has very little intermodel spread, is small compared to the direct radiative effect or uniform ocean warming response, and the piSST decomposition does a relatively good job of decomposing the abrupt-4xCO2 response, by better understanding the spread in the response to the direct radiative effect, uniform SST warming and patterned SST change we are able to better understand the causes of intermodel spread in the wider CMIP6 model ensemble.

In the following sections these components are analysed individually using the larger (13 model) amip experiment based ensemble to investigate the spread in the response to the direct radiative effect and uniform SST warming, and using the 41 member ensemble of abrupt-4xCO2 simulations to investigate the impact of different SST patterns.

b. Intermodel Spread - Direct Radiative Effect

As discussed in Section 1 and summarised in Figure 1a, the direct radiative effect of increased CO_2 causes an increase in WAM precipitation due to a northward shift and a weakening of the shallow meridional circulation, associated with large-scale temperature gradient changes, as well as the more local influence of a soil moisture feedback over the Sahel. Mutton et al. (2022) focused primarily on a single model analysis of HadGEM2-A as well as the CMIP6 ensemble mean. Here, the 13 model ensemble of amip-4xCO2 experiments is analysed and to identify key differences between models that project larger or smaller precipitation changes in response to the direct radiative effect, two groupings of models are used to capture the four weakest and four strongest responses (Figure 3). The strongest 4 ($S4_{4\times CO2}$) group consists of CNRM-CM6-1, HadGEM3-GC31-LL, IPSL-CM6A-LR, and MIROC6, whilst the weakest 4 ($W4_{4\times CO2}$) group consists of GISS-E2-1-G, CESM2, NorESM2-LM, and MRI-ESM2-0.

In this analysis zonal mean responses are investigated and to ensure the results are not swayed by one particular model the group means are calculated 4 times, leaving one model out each time. To test the significance of the difference between the response seen in the two groups a t-test is performed at each latitude, using the response over each time and longitude within the region to capture the spread in the response for each group mean. Performing this t-test for every combination of the three model means from each group we state a difference is only significance if the t-test for

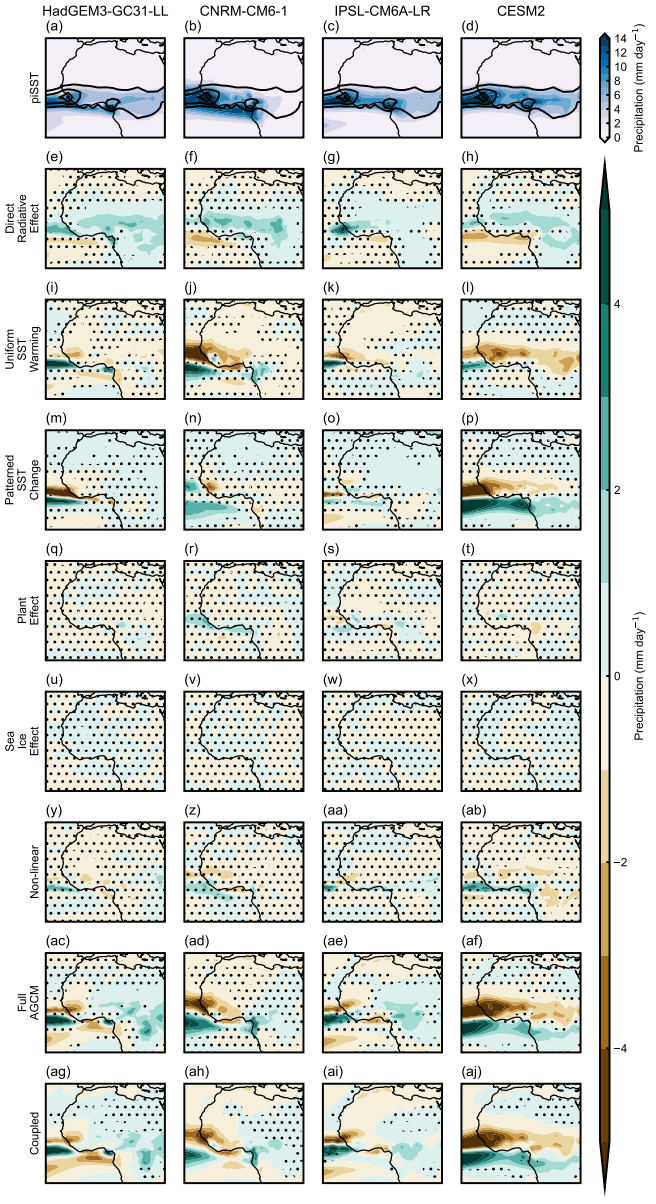

FIG. 4. Maps of JJA precipitation (top row) climatology and (all other panels) anomaly each of the different components of the piSST based decomposition of the full forcing of increased CO_2 (see table 1 and table 2 for a description of the different experiments used). ag, ah, ai, and aj show the coupled model response defined as the difference between abrupt-4xCO2 and piControl experiments. for all panels Stippling is used to indicate where the precipitation anomalies are not significant at the 95% confidence interval. Here a t-test is applied using the null hypothesis that the time-mean of the precipitation anomalies in each location is zero.

every combination produces a p-value below 1%. The analysis here focuses on several of the key processes identified by Mutton et al. (2022), investigating how these processes are simulated in the two model groups and therefore how they contribute to the uncertainty in WAM projections.

The precipitation climatology (amip) and direct radiative effect anomaly (amip-4xCO2 - amip) in the $S4_{4\times CO2}$ and $W4_{4\times CO2}$ groups is presented in Figure 5, there key difference between the two groups can be seen. In the climatology, the models with a stronger response tend to have a precipitation climatology shifted further south, with significantly more precipitation south of 7°N and significantly less precipitation north of 9°N. Comparing these distributions to the GPCP observations, the weaker models do a better job at capturing the northward extent of the rainband but simulate too little precipitation to the south. Comparing the precipitation response to the direct radiative effect, by construction the $S4_{4\times CO2}$ models exhibit larger increases in precipitation. This increase is seen across almost the whole monsoon region whilst the $W4_{4\times CO2}$ models simulate a weaker increase and a dipole type pattern with decreases in precipitation to the south and increases in precipitation to the north. Although previously Monerie et al. (2017), Monerie et al. (2020b) and Yan et al. (2019) find that no relationship exists between climatological biases and future changes, with Monerie et al. (2020b) investigating the biases in coupled historical experiments and the response in the RCP85 scenario, these results show that at least in the case of the response to the direct radiative effect, there may be a relationship between a model's climatology and its response.

In response to the direct radiative effect, the increase in precipitation has been shown to be associated with a northward shift and weakening of the shallow meridional circulation (Mutton et al. 2022). Changes in this shallow circulation can be characterised using the 700hPa horizontal moisture flux divergence with a region of divergence between approximately 15-20°N. Any changes in moisture flux divergence can also be decomposed into dynamic and thermodynamic components (Figure 6).

Climatologically, it can be seen that the $S4_{4\times CO2}$ models have a stronger 700hPa divergence associated with the shallow circulation located slightly further south compared to the $W4_{4\times CO2}$ models (Figure 6a). This is consistent with the climatological precipitation seen in the two groups, with the monsoon rainband in the $S4_{4\times CO2}$ also being located southwards of the $W4_{4\times CO2}$

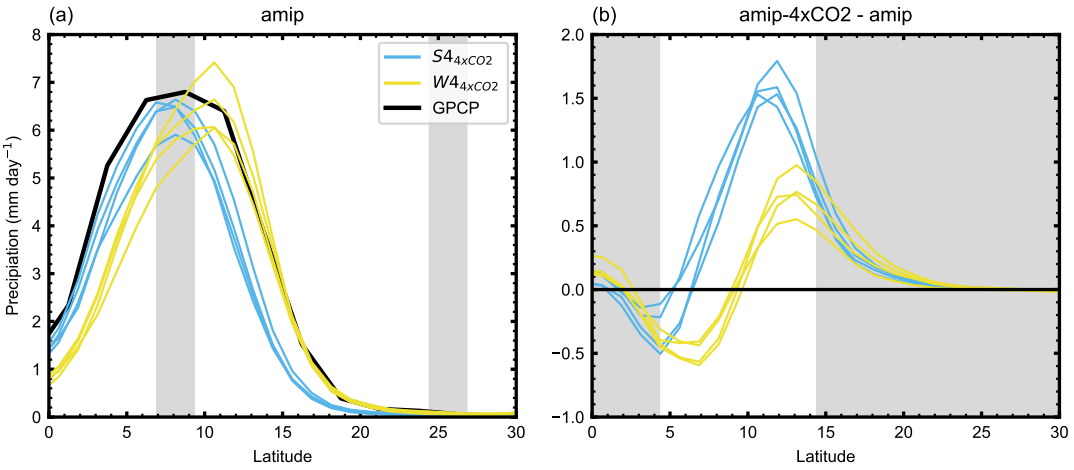

FIG. 5. JJA precipitation averaged between 10°W – 25°E (green dashed lines in Figure 1) for; (a) amip climatology and (b) amip-4xCO2 - amip anomaly in the strongest 4 ($S4_{4\times CO2}$) and weakest 4 ($W4_{4\times CO2}$) models with respect to the magnitude of the direct radiative effect anomaly. Note, the 4 models in each group have been sampled 4 times, missing one model out each time. Therefore each colored line represents an ensemble mean made up of 3 of the 4 models. Grey shading has been used to highlight where the difference between the two groups is not significant at the 1% confidence interval. (a) also shows GPCP observed precipitation averaged between 1979 - 2019.

models. To compare the climatologies in the two groups with observations, horizontal moisture flux divergence has also been calculated using the ERA5 reanalysis (Figure 6a). There the location and magnitude of the maximum divergence in ERA5 more closely matches the $W4_{4xCO2}$.

In response to the direct radiative effect, the $S4_{4\times CO2}$ models have a larger decrease in the shallow circulation strength, and whilst the distribution of anomalous horizontal moisture flux divergence in the $W4_{4\times CO2}$ models is similar, the magnitude of these anomalies are smaller. Comparing the percentage change in total moisture flux divergence associated with the shallow circulation, a -22% change is seen in the $S4_{4\times CO2}$ models and a -17% change is seen in the $W4_{4\times CO2}$ models. Here this total moisture flux divergence change has been estimated averaging between 8-26°N to account for both sides of the dipole seen in the direct radiative effect response, similar to Mutton et al. (2023). Decomposing the total change in horizontal moisture flux divergence into dynamic and thermodynamic components (Figure 6c and d), the dynamic term contributes more to the weakening of the moisture flux divergence in the $W4_{4\times CO2}$ and $S4_{4\times CO2}$ models. However,

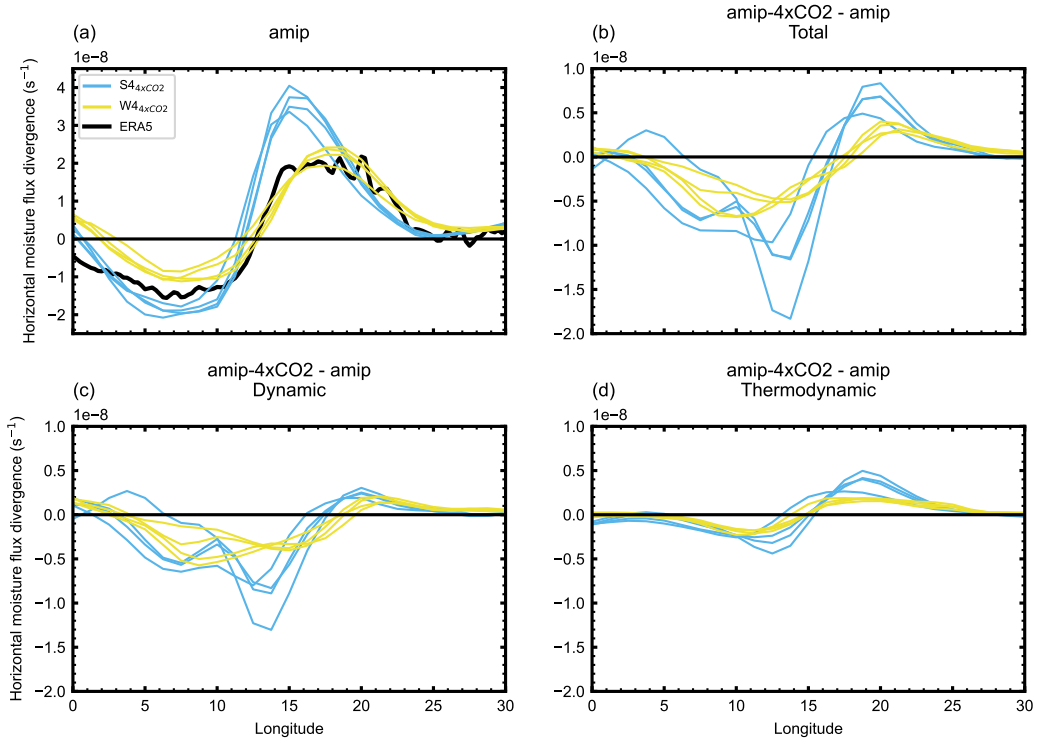

FIG. 6. JJA zonal mean of $S4_{4\times CO2}$ and $W4_{4\times CO2}$; (a) climatological, (b) anomalous (amip-4xCO2 - amip) 700hPa horizontal moisture flux divergence. Climatological horizontal divergence of moisture transport from the ERA5 reanalysis is also shown in (a). The total change in horizontal moisture flux divergence shown in (b) has also been decomposed into; (c) a dynamic component, and (d) a thermodynamic component. Similar to Figure 5, the 4 models in each group have been sampled 4 times, missing one model out each time. Therefore each colored line represents an ensemble mean made up of 3 of the 4 models. Grey shading has been used to highlight where the difference between the two groups is not significant at the 1% confidence interval.

the thermodynamic term here does play a more important role compared to the HadGEM2-A analysis in Mutton et al. (2022). The results presented in Figure 6 demonstrate that the weakening and northward shift of the shallow circulation is strongest in the models with the largest changes in precipitation.

Changes in the shallow meridional circulation have been linked to large-scale temperature gradient changes using Low Level Atmospheric Thickness (LLAT) (Shekhar and Boos 2017), where more warming over the drier desert to the north compared to the monsoon region leads to a northward shift and weakening of the circulation (Mutton et al. 2022). The climatological LLAT

in the $S4_{4\times CO2}$ and $W4_{4\times CO2}$ models is shown in Figure 7a, where both $S4_{4\times CO2}$ and $W4_{4\times CO2}$ models are relatively similar. In response to the direct radiative effect (Figure 7b), the $S4_{4\times CO2}$ and $W4_{4\times CO2}$ models are again similar in the northern part of the domain. However, to the south, the $W4_{4\times CO2}$ models demonstrate a much larger increase in LLAT. This difference means that the large-scale gradient in LLAT is larger for the $S4_{4\times CO2}$ compared to the $W4_{4\times CO2}$ models. The stronger LLAT gradient in the $S4_{4\times CO2}$ models would be expected to lead to a larger change in the shallow circulation and therefore lead to a larger increase in precipitation, as are both seen.

Changes in the shallow meridional circulation have also been shown to be amplified by a soil moisture - surface heat flux feedback over the Sahel (Mutton et al. 2022). In response to the precipitation increase over the Sahel, the surface latent heat flux increases and the surface sensible heat flux decreases. This change in surface heat flux causes the near surface temperatures to cool, acting to locally enhance the large-scale changes in temperature gradient. These temperature changes lead to circulation changes which positively feed back on the initial precipitation change. To demonstrate how this feedback is simulated in the $S4_{4\times CO2}$ and $W4_{4\times CO2}$ models, zonally averaged surface heat fluxes in the amip experiment and the amip-4xCO2 - amip anomaly are shown in Figure 7c, d, e, and f, and air temperature 2m above the surface is shown in Figure 7g and h.

From Figure 7d and f, it is clear that the soil moisture response is much more pronounced in the $S4_{4\times CO2}$ compared to the $W4_{4\times CO2}$, with a strong increase in latent heat flux and a decrease in sensible heat flux. Although the $W4_{4\times CO2}$ models do capture increases in latent heat flux north of 15°N, the decrease in sensible heat is not evident. This result is consistent with the fact that the $S4_{4\times CO2}$ models have a larger increase in precipitation. The $W4_{4\times CO2}$ models also have both the climatological distribution as well as the direct radiative effect anomalies in surface heat fluxes shifted further northwards compared to the $S4_{4\times CO2}$ model (Figure 7c, d, e and f). This is consistent with the results shown in Figure 5 where the climatological precipitation distribution in the $W4_{4\times CO2}$ models also extends further north.

The 2m temperatures respond to these changes in sensible heat flux. Figure 7g and h indicate that both the $S4_{4\times CO2}$ and $W4_{4\times CO2}$ models exhibit similar large-scale climatological and anomalous patterns in 2m temperature with the transition between the cooler monsoon region to the warmer

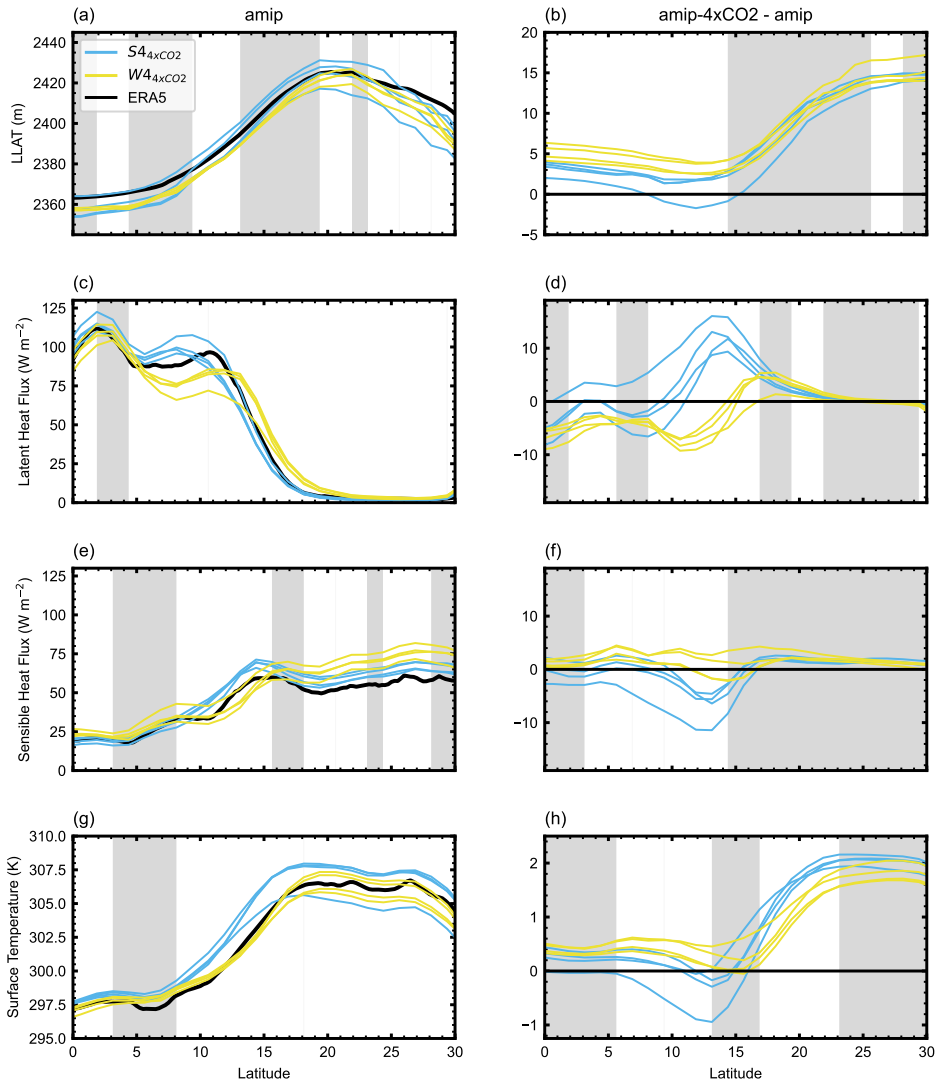

FIG. 7. JJA (a and b) LLAT, (c and d) surface latent heat fluxes, (e and f) surface sensible heat fluxes, and (g and h) 2m temperature in the $S4_{4\times CO2}$ and $W4_{4\times CO2}$ models zonally averaged between 10°W – 25°E in (a, c, e, and g) amip climatology, and (b, d, f, and h) amip-4xCO2 - amip anomaly. Black lines in (a, c, e, and g) show the ERA5 reanalysis JJA climatology. Similar to Figure 5, the 4 models in each group have been sampled 4 times, missing one model out each time. Therefore each colored line represents an ensemble mean made up of 3 of the four models. Grey shading has been used to highlight where the difference between the two groups is not significant at the 1% confidence interval.

Sahara shifted further north in the $W4_{4\times CO2}$ models. In response to the direct radiative effect (Figure 7h), both subsets of models exhibit similar large-scale warming patterns with more warming to

the north compared to the south. The $S4_{4\times CO2}$ models exhibit a larger increase in the large-scale temperature gradient with a smaller warming to the south and a larger warming to the north compared to the $W4_{4\times CO2}$ models. Both $S4_{4\times CO2}$ and $W4_{4\times CO2}$ exhibit a local minima in temperature anomalies associated with the reduction of sensible heat flux, and this acts to locally enhance the large-scale gradient in surface temperatures. The minimum in anomalous temperature seen around 12 - 15°N is stronger in the $S4_{4\times CO2}$ models, meaning that the anomalous temperature gradient to the north of this minimum is larger in the $S4_{4\times CO2}$ models compared to the $W4_{4\times CO2}$ models. This stronger minimum in temperature is consistent with the larger decrease in sensible heat flux in the $S4_{4\times CO2}$ models.

Here the key differences between models that simulate a strong precipitation response to the direct radiative effect and those that simulate a weak response have been investigated. It is demonstrated that the models with a larger precipitation response also exhibit more strongly the mechanisms described in Mutton et al. (2022), including the response of the shallow circulation, the large-scale temperature gradient changes, and the local soil moisture feedback which locally enhances the large-scale temperature gradient anomalies.

c. Intermodel Spread - Uniform Ocean Warming

In response to a uniform ocean warming, the WAM precipitation decreases due to enhanced humidity gradients over the Sahel, increased dry air advection into the monsoon rainband from the north at 700hPa associated with the shallow meridional circulation, and similar to the direct radiative effect mechanisms discussed, a soil moisture - sensible heat flux feedback that acts to amplify any changes in rainfall through circulation changes (Mutton et al. 2023). These processes are summarised in Figure 1b. In this section, the intermodel spread in projections in response to a uniform ocean warming across the 13 member amip based ensemble is investigated. Similar to section 3b, a composite approach is taken, grouping models into the strongest 4 ($S4_{p4K}$) and weakest 4 ($W4_{p4K}$) model responses to the uniform SST warming. The $S4_{p4K}$ being those that project the largest decrease in precipitation and the $W4_{p4K}$ being those that project the smallest decrease. Here the $S4_{p4K}$ models are MIROC6, BCC-CM2-MR, MRI-ESM2-0, and GISS-E2-1-G, and the $W4_{p4K}$ models are NorESM2-LM, TaiESM1, CanESM5 and CESM2. Note that these model groups are not the same as the $W4_{4\times CO2}$ and $S4_{4\times CO2}$ groups used in the previous section.

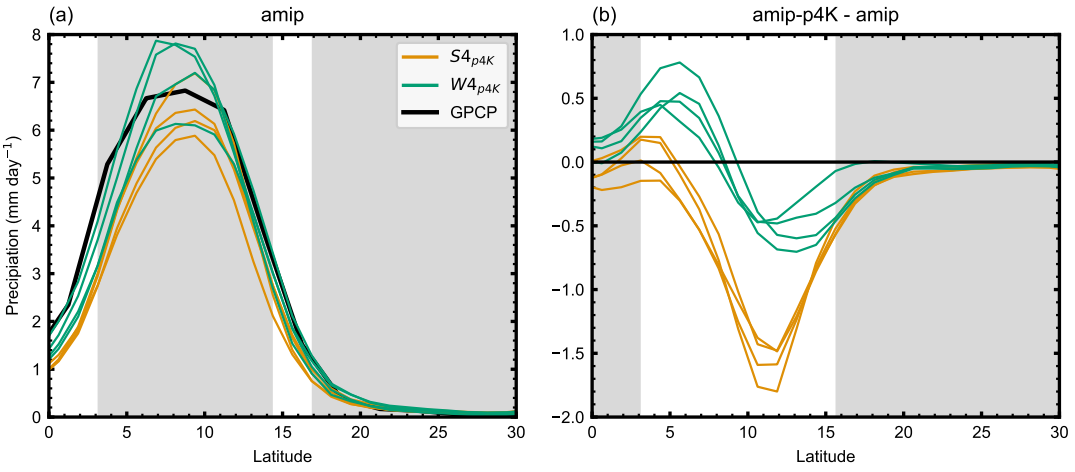

FIG. 8. JJA precipitation averaged between 10°W – 25°E (green dashed lines in Figure 1) for; (a) amip climatology and (b) amip-p4K - amip anomaly in the strongest 4 ($S4_{p4K}$) and weakest 4 ($W4_{p4K}$) models with respect to the magnitude of the precipitation response to a uniform ocean warming. Note, the 4 models in each group have been sampled 4 times, missing one model out each time. Therefore each colored line represents an ensemble mean made up of 3 of the 4 models. Grey shading has been used to highlight where the difference between the two groups is not significant at the 1% confidence interval. (a) also shows GPCP observed precipitation averaged between 1979 - 2019.

The climatological (amip) and anomalous (amip-p4K - amip) precipitation in the $S4_{p4K}$ and $W4_{p4K}$ groups is shown in Figure 8. Climatologically, although the $S4_{p4K}$ models generally have slightly less precipitation compared to the $W4_{p4K}$ models, this difference is not significant. It can also be seen that unlike the $W4_{4\times CO2}$ and $S4_{4\times CO2}$ models, the northward extent of both the climatological monsoon rainband and the response to the uniform ocean warming in the $S4_{p4K}$ and $W4_{p4K}$ models is relatively similar.

In response to a uniform ocean warming, the WAM precipitation reduces due to changes in moisture flux divergence associated with the shallow meridional circulation. Cross-sections of 700hPa horizontal moisture flux divergence climatology and anomaly are shown in Figures 9a and b, with a decomposition of the anomalous moisture flux divergence into dynamic and thermodynamic terms presented in Figures 9c and d. Climatologically, similar to the direct radiative effect, the $S4_{p4K}$ models have a stronger and more distinct shallow circulation. This can be seen in the region of divergence at approximately 17°N. In response to the uniform SST warming, the $S4_{p4K}$ models

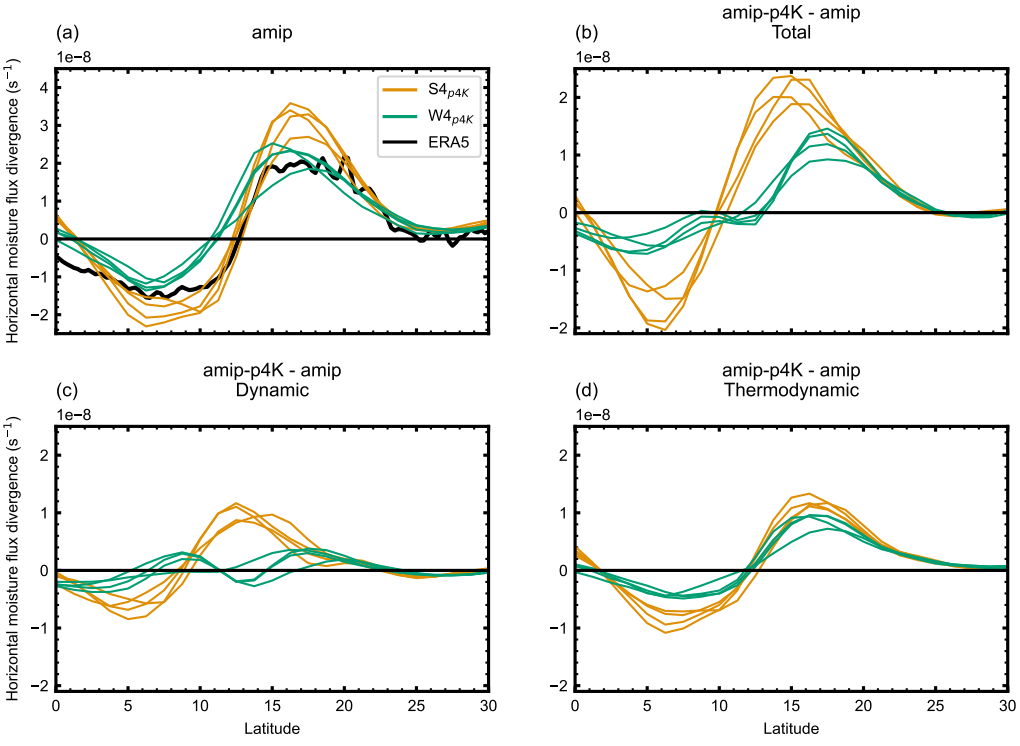

FIG. 9. JJA zonal mean of $S4_{p4K}$ and $W4_{p4K}$; (a) climatological, (b) anomalous (amip-p4K - amip) 700hPa horizontal moisture flux divergence. Climatological horizontal divergence of moisture transport from the ERA5 reanalysis is also shown in (a). The total change in horizontal moisture flux divergence shown in (b) has also been decomposed into; (c) a dynamic component, and (d) a thermodynamic component. Again, the 4 models in each group have been sampled 4 times, missing one model out each time. Therefore each colored line represents an ensemble mean made up of 3 of the 4 models. Grey shading has been used to highlight where the difference between the two groups is not significant at the 1% confidence interval.

also have a greater strengthening of the moisture flux divergence associated with the shallow circulation.

Decomposing these changes in moisture flux divergence into dynamic and thermodynamic terms, in both the $S4_{p4K}$ and $W4_{p4K}$ models, the thermodynamic term is large and relatively consistent in magnitude between the two groups, with a slightly stronger response seen in the $S4_{p4K}$ models. The dynamic term, however, reveals a key difference between the two model groups. There, the $S4_{p4K}$ models exhibit a strengthening of the moisture flux divergence associated with changes in the circulation itself, whereas in the $W4_{p4K}$ models, only very small dynamic changes are seen.

This would suggest that whilst in the $S4_{p4K}$ models the influence of the shallow circulation changes comes from changes in moisture gradients and a strengthening of the circulation, in the $W4_{p4K}$, only the influence of changing moisture gradients are seen, with little changes seen in the circulation itself.

The thermodynamic component of the horizontal moisture flux divergence is caused by a strengthening of the gradient in specific humidity across the Sahel (Mutton et al. 2023; Hill et al. 2017). In response to SST warming, the climatologically moister regions (such as the WAM region) have greater increases in moisture than the climatologically drier regions (such as the Sahara). This differential change in specific humidity between the WAM region and the Sahara leads to an increased gradient in specific humidity and enhances the efficiency with which northerly winds associated with the shallow circulation dry the monsoon rainband and inhibit precipitation. Climatological (amip) and anomalous (amip-p4K - amip) 700hPa specific humidity zonally averaged between 10°W and 25°E is shown in Figure 10g and h. Here, climatologically the $S4_{p4K}$ and $W4_{p4K}$ models have relatively similar specific humidity distributions with the $S4_{p4K}$ models having a slightly higher specific humidity across the transect. In response to the uniform SST warming, the $S4_{p4K}$ models exhibit a much larger increase in specific humidity gradient compared to the $W4_{p4K}$ models, with a significantly larger increase in humidity south of 13°N. This stronger gradient in the $S4_{p4K}$ models explains why the thermodynamic term is larger for these models compared to the $W4_{p4K}$ models in Figure 9.

In Mutton et al. (2023), the changes in horizontal moisture flux divergence were shown to be reinforced by a soil moisture - surface heat flux feedback that acts to amplify changes in precipitation and circulation. As precipitation decreases, surface latent heat flux also decreases and sensible heat flux increases. These changes in sensible heat flux cause anomalous warming at the surface and generate circulation changes that act to positively feedback on the initial precipitation change. This mechanism is investigated in the $S4_{p4K}$ and $W4_{p4K}$ models (Figure 12c, d, e and f). In response to a uniform ocean warming, the $S4_{p4K}$ models exhibit a much larger decrease in latent heat flux and a much larger increase in sensible heat flux compared to the $W4_{p4K}$ models.

The changes in surface heat flux influence the circulation patterns through changes to the atmospheric temperature. The 2m air temperature averaged zonally between 10°W – 25°E in the

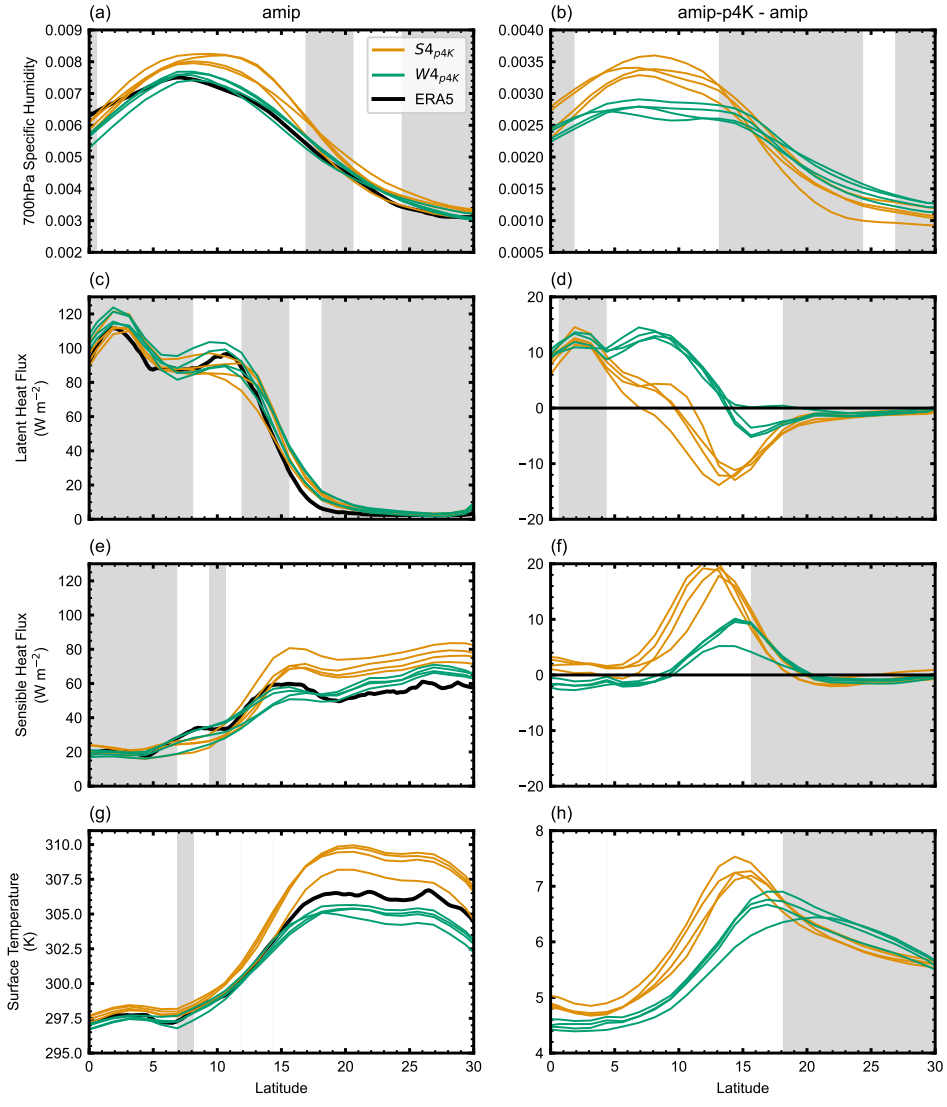

FIG. 10. JJA (a and b) 700hPa specific humidity, (c and d) surface latent heat fluxes, (e and f) surface sensible heat fluxes, and (g and h) 2m temperature in the $S4_{p4K}$ and $W4_{p4K}$ models zonally averaged between 10°W – 25°E in (a, c, e, and g) amip climatology, and (b, d, f, and h) amip-4xCO2 - amip anomaly. Black lines in (a, c, e, and g) show the ERA5 reanalysis JJA climatology. Again, the 4 models in each group have been sampled 4 times, missing one model out each time. Therefore each colored line represents an ensemble mean made up of 3 of the four models. Grey shading has been used to highlight where the difference between the two groups is not significant at the 1% confidence interval.

amip climatology and the uniform SST anomaly is presented in Figure 10e and f. Here, the $S4_{p4K}$ models tend to also have warmer surface temperatures over the whole transect, with particularly

large differences seen over the Sahara in the amip climatology compared to the $W4_{p4K}$. In response to the uniform SST warming, the $S4_{p4K}$ tend to have slightly weaker changes in the large scale temperature gradients, with more warming over the monsoon region and slightly less warming to the north. The largest discrepancy in 2m temperature between the $S4_{p4K}$ and $W4_{p4K}$ models in their response to the uniform SST warming can be seen at around 15°N, in the same location as the maximum in sensible heat flux seen in Figure 12c and d. This suggests that in the $S4_{p4K}$ models, the changes in surface heat fluxes caused by precipitation anomalies are able to influence surface temperature patterns and therefore influence circulation changes. This may also be why the dynamic component of the horizontal moisture flux divergence in the $W4_{p4K}$ is small, since the surface heat flux feedback does not seem to act at all as strongly compared to the $S4_{p4K}$.

The results shown here indicate that the models that exhibit both a stronger enhancement of the meridional gradient in specific humidity, the presence of the soil moisture - surface heat flux feedback, and stronger changes in moisture flux divergence associated with the shallow circulation, also simulate a stronger precipitation decrease in response to a uniform ocean warming. This provides valuable information that can inform our understanding on the large spread seen in the coupled model response to increased CO_2.

d. Intermodel Spread - Patterned SST Change

From Figure 3, it can be seen that the patterned SST change also contributes substantially to the intermodel spread in WAM precipitation projections. In this section, the 4 model ensemble of piSST based timeslice experiments are used to investigate the precipitation changes in response to patterned SST changes, and to explore sources of intermodel spread more robustly, the larger 41 model ensemble of abrupt-4xCO2 simulations is used to apply the metric developed by Giannini et al. (2013) and Guilbert et al. (2024) to investigate intermodel uncertainty.

The 2m temperature climatology (piSST) and anomaly associated with a patterned SST change (a4SST - piSST-pxK) is plotted in Figure 11. Here the variations in SST projections across different models can be seen. Generally, models project a relative warming of the equatorial Atlantic and in the Gulf of Guinea and a relative cooling of the subtropical Atlantic (a pattern particularly prominent in the northern hemisphere in CESM2), consistent with Xie et al. (2010);

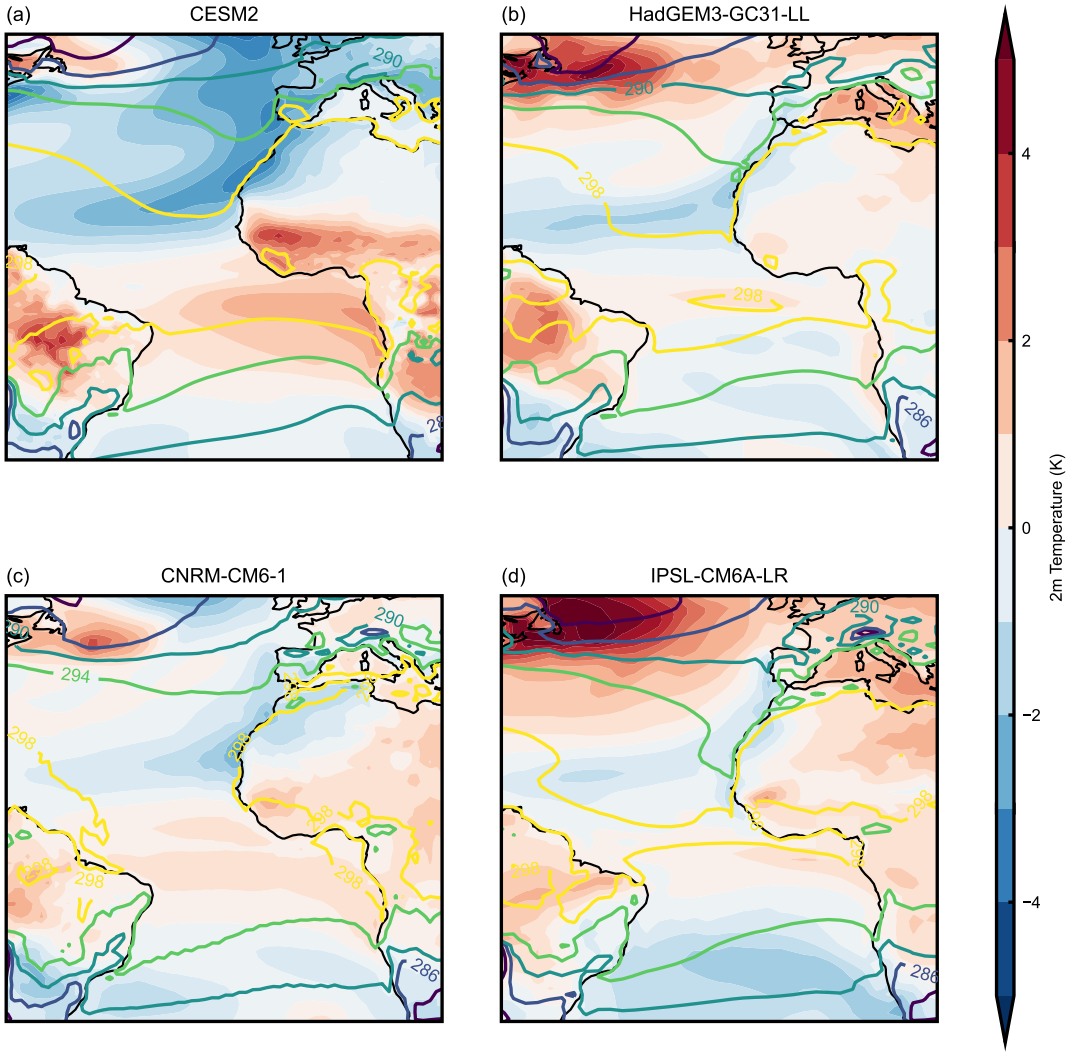

FIG. 11. JJA maps of 2m Temperature piSST climatology (lines) and a4SST - piSST-pxK anomaly associated with a patterned SST change in (a) CESM2, (b) HadGEM3-GC31-LL, (c) CNRM-CM6-1, (d) IPSL-CM6A-LR.

Liu et al. (2005); Leloup and Clement (2009); Vecchi and Soden (2007). IPSL-CM6A-LR and HadGEM3-GC31-LL both have substantial warming over the North Atlantic and the equatorial Atlantic warming extends furthest north in CNRM-CM6-1.

The precipitation response to these SST pattern changes is presented in Figure 4m, n, o, and p. Given each model is being forced by different SST patterns, it is not surprising that the precipitation response to the patterned SST change is highly variable between models. The response over the

ocean is generally for the precipitation to increase over the ocean regions that warm, and to decrease over the ocean regions that cool. This is consistent with the warmer get wetter hypothesis (Xie et al. 2010). CESM2 show this pattern clearly where a strong precipitation dipole is seen between the central Atlantic warming region and the subtropical cooling region. HadGEM3-GC31-LL also exhibits a similar response, only less extreme compared to CESM2, since the SST pattern changes are smaller. CNRM-CM6-1 does not exhibit the precipitation dipole evident in CESM2 and HadGEM3-GC31-LL and instead simulates two precipitation anomaly maxima over the central Atlantic. These maxima are located over two regions of anomalously warm SST indicated in Figure 13. Inland, three of the four models project only relatively small precipitation changes in response to the patterned SST change. The exception to this trend is CESM2, where the precipitation dipole over the central Atlantic extends inland causing a large precipitation decrease over the WAM region and a precipitation increase over central Africa. The precipitation dipole evident in CESM2 and HadGEM3-GC31-LL suggests a southward shift in the oceanic Intertropical Convergence Zone (ITCZ).

Giannini et al. (2013) suggested that the difference between North subtropical Atlantic SSTs and Tropical Mean SSTs is a key metric in capturing WAM precipitation variability (see Figure 2 for the regions used), and Guilbert et al. (2024) explored the influence of inter-hemispheric temperature gradients on WAM uncertainty. We explore the relevance of these two metrics to the uncertainty of WAM projections within the piSST timeslice experiments, and since there are only 4 models within this ensemble, we also investigate the influence of these different SST patterns within the larger CMIP6 ensemble of coupled abrupt-4xCO2 experiments. This enables an estimation of the intermodel spread in the coupled models that is associated with patterned changes to the SSTs. The changes in these indices are plotted against anomalous WAM precipitation for both a4SST - piSST-pxK and abrupt-4xCO2 - piControl experiments (Figure 12). The correlation between the anomalous WAM precipitation and the anomalous Giannini et al. (2013) SST and Guilbert et al. (2024) indices are 0.67 and 0.74 respectively, suggesting a relatively strong influence of both North Atlantic SST patterns and inter-hemispheric temperature gradients on the WAM precipitation. It can also be seen that the SST pattern metrics and WAM precipitation responses seen in the piSST based experiments (a4SST - piSST-pxK) are consistent with the distribution seen in response to the full forcing of increased CO_2 (i.e. abrupt-4xCO2 - piControl). The remainder of the intermodel

Accepted for publication in *Journal of Climate*. DOI 10.1175/JCLI-D-24-0506.1.

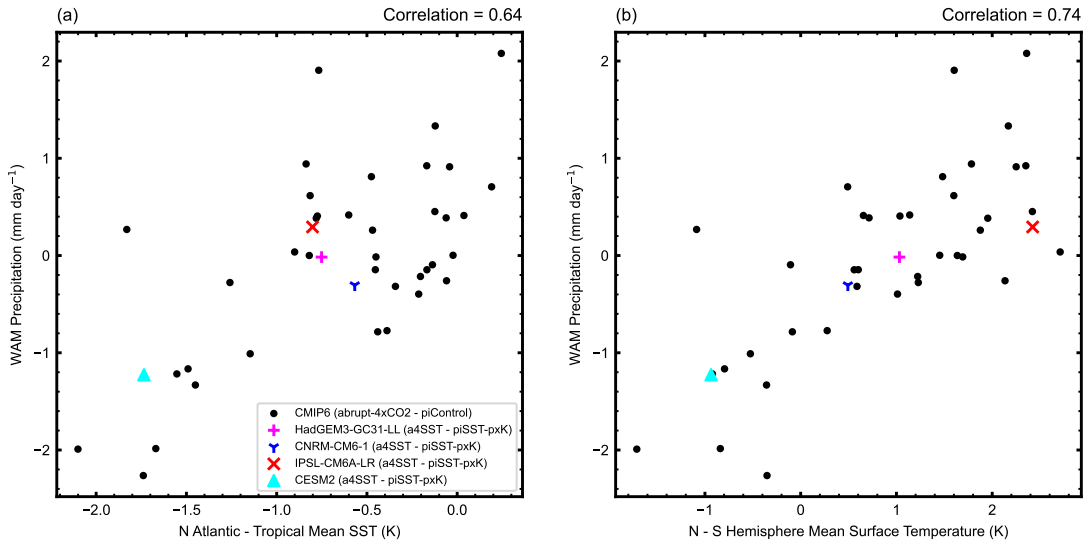

FIG. 12. Scatter plot of anomalous WAM precipitation against; (a) North Atlantic - Tropical mean SSTs, and (b) Northern Hemisphere - Southern Hemisphere mean surface temperatures. 41 model ensemble of abrupt-4xCO2 - piControl is shown in black dots, and anomalies from the a4SST - piSST-pxK are also shown.

spread in the precipitation anomaly is likely associated with the direct radiative effect and the uniform SST warming, together with any other SST pattern influences not correlated with the SST indexes used (e.g. the influence of the Mediterranean (Park et al. 2016)).

4. Discussion and Conclusions

The key sources of uncertainty in the WAM precipitation response to increased CO_2 in the CMIP6 coupled models are found to be the direct radiative effect, the impact of a uniform SST warming, and the impact of a patterned SST change.

The results highlight that in the case of the direct radiative effect and the uniform SST warming, the models that more strongly produce the mechanisms presented in Mutton et al. (2022) and Mutton et al. (2023), also project the strongest changes in precipitation. By grouping the models into the strongest and weakest 4 by their precipitation anomaly, it is possible to show that in response to the direct radiative effect, the models that exhibit a more pronounced weakening and northward shift in the shallow circulation, a larger surface heat flux response, and a greater increase in the large-scale temperature gradient between the WAM region and the Sahara, also project a larger

increase in precipitation. For the response to a uniform SST warming, the models that project a larger strengthening in the shallow circulation, a stronger surface heat flux response, and a greater increase in the large-scale gradient in specific humidity between the WAM region and the Sahara also project a larger decrease in precipitation. Therefore, focusing more work on improving the representation of the shallow circulation and land-surface coupling in models, and on understanding their responses to climate change, could lead to valuable improvements to our projections of future WAM precipitation under increased CO_2. The influence of the shallow circulation shown here is consistent with the findings of Monerie et al. (2020b) who showed that dynamic changes in precipitation contributed more to the intermodel spread compared to thermodynamic changes, and the importance of the soil moisture - surface heat flux feedback seen is consistent with the results of Dosio et al. (2020) who identified different surface heat flux responses as a key difference between models that projected increases or decreases in WAM precipitation.

The intermodel spread in the precipitation response to a patterned SST change has also been investigated. In the timeslice experiments all models exhibit large precipitation anomalies over the ocean with the warmer SSTs associated with increases in precipitation and cooler SSTs associated with decreases in precipitation. Inland however, only one model (CESM2) produces large precipitation anomalies over the WAM region. This model also exhibits the largest cooling of the North Atlantic SSTs which has been shown to cause a decrease in WAM precipitation (Giannini et al. 2013). Since only 4 models produced the timeslice analysis, the intermodel spread in projections associated with a patterned SST change is investigated further in an ensemble of coupled models using the piControl and abrupt-4xCO2 experiments. Using indices developed by Giannini et al. (2013) and Guilbert et al. (2024), it is shown that changes in WAM precipitation are moderately well correlated (correlation coefficient of 0.67 and 0.74 respectively) with these indices. This result suggests that the correct simulation of SSTs in climate models is of great importance if accurate climate projections of WAM precipitation are to be produced.

Although this analysis does give useful insight into the key sources of uncertainty in the coupled model response to increased CO_2, there are a few limitations. The first of these limitations is regarding the ensemble size of both the amip based decomposition (13), and the piSST based timeslice decomposition (4 models). The small ensemble size makes it difficult to find robust and

significant correlations when investigating the intermodel spread. This limitation is particularly present when analysing the patterned SST change using the timeslice experiments. The use of the coupled models in this analysis is useful. However given that in the abrupt-4xCO2 experiment, the influence of the direct radiative effect and the uniform SST warming are also present, the analysis would be improved if a similarly large ensemble could be used with the timeslice experiment setup, where only the impact of the patterned SST change is investigated.

The analysis presented here also highlights areas for future work. One result not fully explored is the possible relationship between a models climatological bias and its response to different components of the response to increased CO_2. Although previously Monerie et al. (2017) and Monerie et al. (2020b) found no relationship exists between climatological biases and future changes, this was investigated in the coupled model response in the RCP85 scenario. Therefore, the possibility that the response to different components of the full forcing to increased CO_2 (e.g. the direct radiative effect or a uniform ocean warming) may be constrained by climatological biases cannot be ruled out.

As well as larger ensembles providing a useful path for further analysis, new experimental designs could also help improve our understanding of changes in WAM precipitation. For example, the SST patterns from each coupled model could be used to prescribe SSTs in a single model analysis to investigate how different potential SST pattern changes would effect the WAM in the absence of the direct radiative effect or a uniform ocean warming, similar to Zhang et al. (2018). This could help separate the uncertainty in projections sourced from the different SST patterns from different model responses to the same SST pattern change. As well as this, another useful path for future work would be to try to understand whether the models WAM response to a certain SST pattern is consistent with the real world. This could be done by finding periods in observations where SST patterns have looked like those seen in the models response to increased CO_2 and looking to see if a similar precipitation change was observed in response to those SSTs. Given SST patterns may also vary strongly with internal variability, utilising larger ensembles to disentangle the influence of internal variability and the forced SST pattern change would also be useful.

Acknowledgments. Harry Mutton was supported by the Met Office Hadley Centre Climate Programme funded by DSIT. Matthew Collins, and F. Hugo Lambert were supported by NERC NE/S004645/1. Chris Taylor was supported by the African Monsoon Multidisciplinary Analysis-2050 project (grant NE/M020428/1). Ruth Geen was supported by the Natural Environment Research Council (grant NE/X014827/1) . Thanks to Brian Medeiros for producing the CESM2 piSST based timeslice experiments used in the analysis, and thanks also to the anonymous reviewers for their helpful comments and suggestions that have greatly helped to improve this manuscript.

Data availability statement. Data used in this analysis consists of model simulations performed for CMIP6 Eyring et al. (2016) and can be accessed from the ESGF CEDA data node https://esgf-index1.ceda.ac.uk/search/cmip6-ceda/.

References

Akinsanola, A., and W. Zhou, 2020: Understanding the variability of West African summer monsoon rainfall: Contrasting tropospheric features and monsoon index. *Atmosphere*, **11**, https://doi.org/10.3390/atmos11030309.

Bellomo, K., M. Angeloni, S. Corti, and J. v. Hardenberg, 2021: Future climate change shaped by inter-model differences in atlantic meridional overturning circulation response. *nature communications*, **12**, https://doi.org/10.1038/s41467-021-24015-w.

Biasutti, M., 2013: Forced Sahel rainfall trends in the CMIP5 archive. *Journal of Geophysical Research: Atmospheres*, **118**, 1613–1623, https://doi.org/doi:10.1002/jgrd.50206.

Biasutti, M., 2019: Rainfall trends in the African Sahel: Characteristics, processes, and causes. *Wiley Interdisciplinary Reviews: Climate Change*, **10**, https://doi.org/10.1002/wcc.591.

Chadwick, R., D. Ackerley, T. Ogura, and D. Dommenget, 2019: Separating the Influences of Land Warming, the Direct CO2 Effect, the Plant Physiological Effect, and SST Warming on Regional Precipitation Changes. *Journal of Geophysical Research: Atmospheres*, **124**, 624–640, https://doi.org/10.1029/2018JD029423.

Accepted for publication in *Journal of Climate*. DOI 10.1175/JCLI-D-24-0506.1.

Chadwick, R., H. Douville, and C. Skinner, 2017: Timeslice experiments for understanding regional climate projections: applications to the tropical hydrological cycle and European winter circulation. *Climate Dynamics*, **49**, 3011–3029, https://doi.org/10.1007/s00382-016-3488-6.

Chadwick, R., P. Good, and K. Willett, 2016: A simple moisture advection model of specific humidity change over land in response to SST warming. *Journal of Climate*, **29**, 7613–7632, https://doi.org/10.1175/JCLI-D-16-0241.1.

Cook, K., and E. Vizy, 2019: Contemporary Climate Change of the African Monsoon Systems. *Current Climate Change Reports*, **5**, 145–159, https://doi.org/10.1007/s40641-019-00130-1.

Dosio, A., and Coauthors, 2020: A tale of two futures: contrasting scenarios of future precipitation for West Africa from an ensemble of regional climate models. *Environmental Research Letters*, **15**, https://doi.org/10.1088/1748-9326/ab7fde.

Endo, H., and A. Kitoh, 2014: Thermodynamic and dynamic effects on regional monsoon rainfall changes in a warmer climate. *Geophysical Research Letters*, **41**, 1704–1710, https://doi.org/10.1002/2013GL059158.

Eyring, V., S. Bony, G. Meehl, C. Senior, B. Stevens, R. Stouffer, and K. Taylor, 2016: Overview of the Coupled Model Intercomparison Project Phase 6 (CMIP6) experimental design and organization. *Geoscientific Model Development*, **9**, 1937–1958, https://doi.org/10.5194/gmd-9-1937-2016.

Gaetani, M., C. Flamant, S. Bastin, S. Janicot, C. Lavaysse, F. Hourdin, P. Braconnot, and S. Bony, 2017: West African monsoon dynamics and precipitation: the competition between global SST warming and CO2 increase in CMIP5 idealized simulations. *Climate Dynamics*, **48**, 1353–1373, https://doi.org/10.1007/s00382-016-3146-z.

Giannini, A., S. Salack, T. Lodoun, A. Ali, A. T. Gaye, and O. Ndiaye, 2013: A unifying view of climate change in the Sahel linking intra-seasonal, interannual and longer time scales. *Environmental Research Letters*, **8**, https://doi.org/10.1088/1748-9326/8/2/024010.

Gong, C., and E. Eltahir, 1996: Sources of moisture for rainfall in west Africa. *Water Resources Research*, **32**, 3115–3121, https://doi.org/10.1029/96WR01940.

Guilbert, M., P. Terray, J. Mignot, L. Ollier, and G. Gastineau, 2024: Interhemispheric temperature gradient and equatorial pacific ssts drive sahel monsoon uncertainties under global warming. *Journal of Climate*, **37**, 1033 – 1052, https://doi.org/10.1175/JCLI-D-23-0162.1.

Held, I. M., T. L. Delworth, J. Lu, K. L. Findell, and T. R. Knutson, 2005: Simulations of Sahel drought in the 20th and 21st centuries. *PNAS*, **102**, 17 891–17 896, https://doi.org/10.1073/pnas.0509057102.

Hill, S. A., Y. Ming, I. M. Held, and M. Zhao, 2017: A moist static energy budget-based analysis of the Sahel rainfall response to uniform oceanic warming. *Journal of Climate*, **30**, 5637–5660, https://doi.org/10.1175/JCLI-D-16-0785.1.

Johnson, N., and S. Xie, 2010: Changes in the sea surface temperature threshold for tropical convection. *Nature Geoscience*, **3**, 842–845, https://doi.org/10.1038/ngeo1008.

Katzenberger, A., J. Schewe, J. Pongratz, and A. Levermann, 2021: Robust increase of indian monsoon rainfall and its variability under future warming in cmip6 models. *Earth System Dynamics*, **12**, 367–386, https://doi.org/10.5194/esd-12-367-2021.

Lavaysse, C., C. Flamant, S. Janicot, D. J. Parker, J.-P. Lafore, B. Sultan, and J. Pelon, 2009: Seasonal evolution of the West African heat low: A climatological perspective. *Climate Dynamics*, **33**, 313–330, https://doi.org/10.1007/s00382-009-0553-4.

Lele, M., L. Leslie, and P. Lamb, 2015: Analysis of low-level atmospheric moisture transport associated with the West African monsoon. *Journal of Climate*, **28**, 4414–4430, https://doi.org/10.1175/JCLI-D-14-00746.1.

Leloup, J., and A. Clement, 2009: Why is there a minimum in projected warming in the tropical North Atlantic Ocean? *Geophysical Research Letters*, **36**, https://doi.org/10.1029/2009GL038609.

Liu, Z., S. Vavrus, F. He, N. Wen, and Y. Zhong, 2005: Rethinking Tropical Ocean Response to Global Warming: The Enhanced Equatorial Warming. *Journal of Climate*, **18**, 4684–4700, https://doi.org/10.1175/JCLI3579.1.

Accepted for publication in *Journal of Climate*. DOI 10.1175/JCLI-D-24-0506.1.

Masson-Delmotte, V., and Coauthors, 2021: *Working Group I Contribution to the Sixth Assessment Report of the Intergovernmental Panel on Climate Change*. IPCC, https://doi.org/10.1017/9781009157896.

Monerie, P., E. Sanchez-Gomez, and J. Boe, 2017: On the range of future sahel precipitation projections and the selection of a sub-sample of cmip5 models for impact studies. *Climate Dynamics*, **48**, 2751–2770, https://doi.org/10.1007/s00382-016-3236-y.

Monerie, P., E. Sanchez-Gomez, M. Gaetani, E. Mohino, and B. Dong, 2020a: Future evolution of the Sahel precipitation zonal contrast in CESM1. *Climate Dynamics*, **55**, 2801–2821, https://doi.org/10.1007/s00382-020-05417-w.

Monerie, P., C. Wainwright, M. Sidibe, and A. Akinsanola, 2020b: Model uncertainties in climate change impacts on Sahel precipitation in ensembles of CMIP5 and CMIP6 simulations . *Climate Dynamics*, **55**, 1385–1401, https://doi.org/10.1007/s00382-020-05332-0.

Monerie, P.-A., M. Biasutti, J. Mignot, E. Mohino, B. Pohl, and G. Zappa, 2023: Storylines of sahel precipitation change: Roles of the north atlantic and euro-mediterranean temperature. *Journal of Geophysical Research: Atmospheres*, **128**, https://doi.org/10.1029/2023JD038712.

Mutton, H., R. Chadwick, M. Collins, F. H. Lambert, R. Geen, A. Todd, and C. Taylor, 2022: The impact of the direct radiative effect of increased CO2 on the West African Monsoon. *Journal of Climate*, **35**, 2441–2458, https://doi.org/10.1175/JCLI-D-21-0340.1.

Mutton, H., R. Chadwick, M. Collins, F. H. Lambert, R. Geen, A. Todd, and C. Taylor, 2023: The impact of a uniform ocean warming on the West African monsoon. *Climate Dynamics*, https://doi.org/10.1007/s00382-023-06898-1.

Park, J.-Y., J. Bader, and D. Matei, 2015: Northern-hemispheric differential warming is the key to understanding the discrepancies in the projected sahel rainfall. *nature communications*, **6**, https://doi.org/10.1038/ncomms6985.

Park, J.-Y., J. Bader, and D. Matei, 2016: Anthropogenic mediterranean warming essential driver for present and future sahel rainfall. *nature climate change*, **6**, https://doi.org/10.1038/nclimate3065.

Accepted for publication in *Journal of Climate*. DOI 10.1175/JCLI-D-24-0506.1.

Raj, J., H. Bangalath, and G. Stenchikov, 2019: West African Monsoon: current state and future projections in a high-resolution AGCM . *Climate Dynamics*, **52**, 6441–6461, https://doi.org/10.1007/s00382-018-4522-7.

Sahastrabuddhe, R., S. A. Ghausi, J. Joseph, and S. Ghosh, 2023: Indian summer monsoon rainfall in a changing climate: a review. *Journal of Water and Climate Change*, **14**, 1061–1088, https://doi.org/10.2166/wcc.2023.127.

Seager, R., H. Liu, N. Henderson, I. Simpson, C. Kelley, T. Shaw, Y. Kushnir, and M. Ting, 2014: Causes of increasing aridification of the mediterranean region in response to rising greenhouse gases. *Journal of Climate*, **27**, 4655 – 4676, https://doi.org/10.1175/JCLI-D-13-00446.1.

Shekhar, R., and W. R. Boos, 2017: Weakening and Shifting of the Saharan Shallow Meridional Circulation during Wet Years of the West African Monsoon . *Journal of Climate*, **30**, 7399–7422, https://doi.org/10.1175/JCLI-D-16-0696.1.

Vecchi, G., and B. Soden, 2007: Effect of remote sea surface temperature change on tropical cyclone potential intensity. *Nature*, **450**, https://doi.org/10.1038/nature06423.

Wang, B., and Q. Ding, 2006: Changes in global monsoon precipitation over the past 56 years. *Geophysical Research Letters*, **33**, https://doi.org/10.1029/2005GL025347.

Webb, M. J., and Coauthors, 2017: The Cloud Feedback Model Intercomparison Project (CFMIP) contribution to CMIP6. *Geoscientific Model Development*, **10**, 359–384, https://doi.org/10.5194/gmd-10-359-2017.

Xie, S.-P., C. Deser, G. A. Vecchi, J. Ma, H. Teng, and A. T. Wittenberg, 2010: Global Warming Pattern Formation: Sea Surface Temperature and Rainfall. *Journal of Climate*, **23**, 966–986, https://doi.org/10.1175/2009JCLI3329.1.

Yan, Y., R. Lu, and C. Li, 2019: Relationship between the future projections of sahel rainfall and the simulation biases of present South Asian and western North Pacific rainfall in summer . *Journal of Climate*, **32**, 1327–1343, https://doi.org/10.1175/JCLI-D-17-0846.1.

Zhang, G., D. S. Nolan, C. D. Thorncroft, and H. Nguyen, 2008: Shallow meridional circulations in the tropical atmosphere. *Journal of Climate*, **21**, 3453–3470, https://doi.org/10.1175/2007JCLI1870.1.

Zhang, H., Y. Zhao, A. Moise, H. Ye, R. Colman, G. Roff, and M. Zhao, 2018: On the influence of simulated sst warming on rainfall projections in the indo-pacific domain: an agcm study. *Climate Dynamics*, **50**, 1373–1391, https://doi.org/10.1007/s00382-017-3690-1.

Accepted for publication in *Journal of Climate*. DOI 10.1175/JCLI-D-24-0506.1.